

Anomalously large spin-dependent electron correlation in the nearly half-metallic ferromagnet CoS₂

Hirokazu Fujiwara ^{1,2,*}, Kensei Terashima,³ Junya Otsuki ⁴, Nayuta Takemori ⁴, Harald O. Jeschke ⁴, Takanori Wakita,⁴ Yuko Yano,¹ Wataru Hosoda,¹ Noriyuki Kataoka ¹, Atsushi Teruya,⁵ Masashi Kakihana,⁵ Masato Hedo,⁶ Takao Nakama,⁶ Yoshichika Ōnuki,^{6,7} Koichiro Yaji ³, Ayumi Harasawa ², Kenta Kuroda,² Shik Shin,² Koji Horiba ⁸, Hiroshi Kumigashira ⁸, Yuji Muraoka ^{1,4} and Takayoshi Yokoya ^{1,4,†}

¹Graduate School of Natural Science and Technology, Okayama University, Okayama 700-8530, Japan

²Institute for Solid State Physics, The University of Tokyo, Kashiwa, Chiba 277-8581, Japan

³National Institute for Materials Science (NIMS), Tsukuba, Ibaraki 305-0044, Japan

⁴Research Institute for Interdisciplinary Science, Okayama University, Okayama 700-8530, Japan

⁵Graduate School of Engineering and Science, University of the Ryukyus, Nishihara, Okinawa 903-0213, Japan

⁶Faculty of Science, University of the Ryukyus, Nishihara, Okinawa 903-0213, Japan

⁷RIKEN Center for Emergent Matter Science, Wako, Saitama 351-0198, Japan

⁸Photon Factory, Institute of Materials Structure Science, High Energy Accelerator Research Organization (KEK), 1-1 Oho, Tsukuba 305-0801, Japan



(Received 7 December 2021; revised 13 June 2022; accepted 19 July 2022; published 9 August 2022)

The spin-dependent band structure of CoS₂, which is a candidate for a half-metallic ferromagnet, was investigated by both spin- and angle-resolved photoemission spectroscopy and theoretical calculations to reappraise the half-metallicity and electronic correlations. We determined the three-dimensional Fermi surface and the spin-dependent band structure. As a result, we found that a part of the minority spin bands is on the occupied side in the vicinity of the Fermi level, providing spectroscopic evidence that CoS₂ is not a half-metal but very close. Band calculations using density functional theory with generalized gradient approximation showed good agreement with the observed majority spin e_g bands, while it could not explain the observed band width of the minority-spin e_g bands. On the other hand, theoretical calculations using dynamical mean field theory could better reproduce the strong mass renormalization in the minority-spin e_g bands. Our results strongly suggest the presence of anomalously enhanced spin-dependent electron correlation effects on the electronic structure in the vicinity of the half-metallic state. We also report the temperature dependence of the electronic structure across the Curie temperature and discuss the mechanism of the thermal demagnetization. Our discovery of the anomalously large spin-dependent electronic correlations not only demonstrates a key factor in understanding the electronic structure of half-metals but also provides a motivation to improve theoretical calculations on spin-polarized strongly correlated systems.

DOI: [10.1103/PhysRevB.106.085114](https://doi.org/10.1103/PhysRevB.106.085114)

I. INTRODUCTION

Producing a source of spin-polarized carriers has been a challenging topic of research in solid state physics since the emergence of spintronics which manipulates the spin degree of freedom of carriers [1,2]. Efforts to realize carriers with large spin polarization have been vigorously undertaken in studies on half-metallic ferromagnets (HMFs) [3–7]. HMFs have metallic electronic structures with an energy gap at the Fermi level (E_F) for any one electronic spin state in the ground state, realizing 100% spin polarization at E_F [8]. Although many HMF candidates have been predicted for transition metal oxides and chalcogenides, Heusler alloys, and two-dimensional materials [9–13], CrO₂ has been the sole substance providing $\sim 100\%$ spin polarization in both point-contact Andreev reflection (PCAR) and spin-resolved

photoemission spectroscopy experiments [14–18]. Further discovery and identification of half-metallic materials is necessary to understand characteristic phenomena of HMFs and to realize more thermally stable HMFs.

In CrO₂, there are two claims on electron correlation: a soft x-ray angle-resolved photoemission spectroscopy (SXARPES) study shows that the observed majority spin band is very well explained by dynamical mean-field theory (DMFT) calculations assuming a small effective local Coulomb repulsion $U_{\text{eff}} < 1$ eV [19]. On the other hand, in spin-resolved photoemission spectroscopy reports, the temperature dependence of the minority spin state near E_F provides evidence that strong correlation effects are critical for understanding the electronic structure of CrO₂ [17,18]. Although these claims seem to be contradictory, they can be interpreted consistently by assuming the existence of spin-dependent electron correlation. This spin-dependent electron correlation is expected to be a universal effect in ferromagnets, but few previous studies have investigated the effect [20–22]. In CrO₂, it is difficult to investigate both majority and

*hfujwara@issp.u-tokyo.ac.jp

†yokoya@cc.okayama-u.ac.jp

minority spin bands simultaneously because there is no occupied minority spin band at E_F at low temperatures.

CoS_2 is a ferromagnetic metal whose ordered moment is reported to be $\sim 0.9 \mu_B/\text{Co}$ with an easy-axis along the [111] direction [23–25]. The ordered moment is $\sim 1 \mu_B/\text{Co}$ in a low-spin state of Co^{2+} (configuration: $t_{2g}^6 e_g^1$), suggesting that CoS_2 has a half-metallic electronic structure including completely spin-polarized e_g bands crossing E_F . The half-metallicity has also been supported by theoretical band structure calculated within generalized gradient approximation (GGA), an experimental study of the de Haas–van Alphen (dHvA) effect, and an optical study measuring reflectivity of CoS_2 [10,24,26]. On the other hand, the results of band calculations within local spin-density approximation (LSDA), PCAR, x-ray magnetic circular dichroism, and photoemission spectroscopy measurements indicated that CoS_2 has a nearly half-metallic electronic structure in which the bottom of the lowest-energy minority spin e_g band touches E_F or is slightly occupied near the R point [10,27–32]. This band-structure picture is also supported by the angle-resolved photoemission spectroscopy (ARPES) study on CoS_2 [33] and PCAR studies on $\text{Co}_{1-x}\text{Fe}_x\text{S}_2$. In this system, the spin polarization at E_F is enhanced by hole doping [34,35]. In a polarized neutron-diffraction study, a non-half-metallic electronic state was inferred from the observed magnetization distribution, in which both e_g and t_{2g} states contributed to the magnetic moments [36]. This conflicts with the physical picture obtained by photoemission spectroscopy and density functional theory (DFT) studies based on LSDA [31–33]. So far, there is still no consensus on the half-metallicity of CoS_2 . Therefore, a direct observation of the spin-dependent electronic structure is required. If CoS_2 has an occupied minority spin band near E_F , we can observe both majority and minority spin bands simultaneously and discuss spin-dependent mass renormalization.

To reveal the spin-resolved electronic structure of CoS_2 experimentally, it has been pointed out that measurements with energy resolution < 10 meV are needed. A photoemission study demonstrated that the peak width of a structure attributed to a minority spin state was 6.5 meV [28]. Clarifying the fine electronic structure with spin character can provide the decisive evidence for the half-metallicity of CoS_2 .

In this paper, we report on the three-dimensional Fermi surface (FS) and the band structure of CoS_2 single crystals including the spin character determined by high-resolution spin- and angle-resolved photoemission spectroscopy (SARPES). We have found that both majority and minority spin bands cross E_F along the ΓX line, unambiguously demonstrating that CoS_2 does not have a half-metallic electronic structure down to 20 K. Furthermore, the minority spin bands are renormalized by electron correlation effects, while the overall character of the majority spin band can be understood by the one-electron model. This indicates that spin-dependent electron correlation is important for understanding the electronic structure of CoS_2 . Based on the experimentally determined electronic structure, we discuss (i) the half-metallicity in Secs. II A and II B, (ii) the spin-dependent electron correlation effects from comparison with band structures computed in DFT based on GGA and in combination with DMFT (DFT + DMFT) in Secs. II C and II D, (iii) the demagnetization process and the thermal decoherence of near- E_F bands

in Sec. II E, and finally, (iv) possible origins of the spin-dependent electron correlation in CoS_2 in Sec. II F.

II. RESULTS AND DISCUSSION

A. Three-dimensional FS and spectral function

The photoemission spectroscopy measurements were performed for a cleaved surface of a CoS_2 single crystal. The low-energy electron diffraction (LEED) pattern is shown in Fig. 1(a). Figures 1(c)–1(f) show the experimental in-plane FSs for the cut P1 and P2 which are defined in Fig. 1(b). By determining the Fermi wave vectors (k_F) and using twofold symmetrization analysis [Figs. 1(e)–1(h)], we found two large sheets and a pocket around the Γ point (α , β , and γ , respectively), one pocket around the X' point, and one pocket around the M point in the cut P1.

Figures 2(a) and 2(b) show the observed spectra along the ΓX line. As shown in Fig. 2(a), we observed a peak structure located at $E - E_F = -1.0$ eV, which is accompanied by another structure at -0.75 eV [Fig. 2(b)] corresponding to the exchange-split t_{2g} bands. Furthermore, we observed bands dispersing between -0.5 eV and E_F corresponding to the e_g bands. A dispersive band with a bottom at -0.5 eV near the Γ point was observed along the in-plane k_x direction [Fig. 2(b)]. This band was also observed in a previous ARPES study [33]. Around the X point, we found that the higher intensity near E_F consists of several bands as indicated by polarization-dependent measurements [Figs. 2(c) and 2(d)]. The band with a bottom around the Γ point, which forms the FS named α , crosses E_F around X [Figs. 2(c) and 2(d), circularly polarized and s polarized]. Although the intensity derived from a hole band, which forms the FS named β , is quite small for the circularly polarized light, it becomes clearer for the p -polarized light, as shown in the right panel in Figs. 2(c) and 2(d), because of an orbital selectivity of photoexcitation [37,38]. In addition, we found heavy bands located just below E_F , which we call γ and δ . Based on these results, we summarize the band structure in Figs. 2(e) and 2(f). Along the ΓX line, the α , β , and γ bands cross E_F and constitute the FSs. Comparing our experimental electronic structure with the published theoretical band structure [27], the β band is assigned to a majority spin hole band forming a hole FS around the Γ point. The α band also corresponds to a majority spin band around the Γ point. The experimental α band, however, crosses E_F although the corresponding theoretical band does not cross E_F . Furthermore, there is seemingly no theoretical band in the occupied states to which we can assign the γ and δ bands. To clarify the character of the γ and δ bands, we investigated the spin-resolved band structure by high-resolution SARPES, as described below.

B. Spin-resolved electronic structure

Our high-resolution SARPES results are summarized in Fig. 3. Using $h\nu = 6.994$ eV, the measured k_x line is in the $\Gamma X M X'$ plane, as shown in Fig. 3(a). We observed an ellipsoidal FS around the Γ point and a linear FS along the k_y direction at $k_x = 0.33 \text{ \AA}^{-1}$, as shown in Fig. 3(b), which corresponds to γ and β , respectively, defined in Fig. 1(e). Figures 3(c)–3(h) show SARPES intensity maps taken along

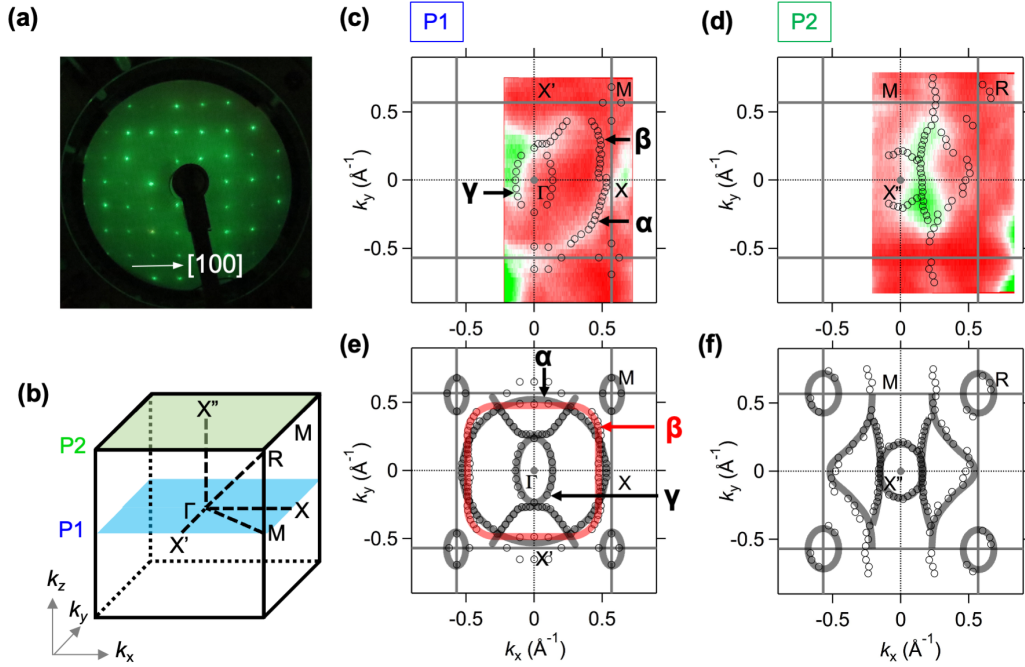


FIG. 1. (a) Low-energy electron diffraction (LEED) pattern at an incident electron energy of 185 eV. (b) Brillouin zone of pyrite-type CoS₂. (c) and (d) Angle-resolved photoemission spectroscopy (ARPES) intensity maps of the Fermi surface (FS) measured at $h\nu = 66$ and 87 eV [corresponding to cuts P1 and P2 marked in (b)], respectively, overlaid with the fitted momentum distribution curve (MDC) peak positions at $E = E_F$ showing the k_F positions (black circles). (e) and (f) k_F plots along P1 and P2, respectively, symmetrized by assuming a twofold symmetry with respect to the Γ point. The thick shaded lines are guides for the eye.

the blue line in Fig. 3(b). We observed bands located at $E - E_F = -1$ eV, -0.5 eV, and -50 meV, just below E_F , and a dispersive hole band corresponding to the β band. From Fig. 3(i), the bands located at -1 eV split into majority (lower energy) and minority (higher energy) spin bands, as marked by black solid lines. These spectral features strongly support the picture shown by GGA calculations that the t_{2g} bands split into the majority and minority spin bands [10].

For the e_g bands, we obtained the spin-polarized band structure more clearly. From the correspondence to the band structure obtained by our ARPES measurements, we identified the e_g bands, as shown in Figs. 3(c) and 3(f). At $E - E_F = -0.5$ eV, the SARPES intensity map for the majority spin character has a clear structure corresponding to the bottom of the α band shown in Fig. 2(c), although the map for the minority spin bands has no structure at -0.5 eV. In the same way, it is ascertained that the β band has majority spin character. The result that the spin character of the α and β bands corresponds to the majority spin is consistent with the band structures calculated within GGA [10]. On the other hand, the γ and δ bands have minority spin character, as clearly shown in Fig. 3(e). We discuss detailed characteristics and interpretation of the minority spin bands below.

Here, we discuss the half-metallicity of CoS₂. As bands forming FSs, we observed not only the majority spin bands but also the minority spin bands, as shown in Figs. 3(c)–3(h). The minority spin bands are occupied only down to 100 meV binding energy, providing spectroscopic evidence for near rather than true half-metallicity of CoS₂. The minority spin bands are

present down to 20 K, as shown later. This result is consistent with claims by Andreev reflection and photoemission studies [29,31,32]. The non-half-metallicity is also supported by the fact that the ordered moment $\mu_s \sim 0.9 \mu_B/\text{Co}$ at 2 K [23,24] is not exactly $\mu_s = 1 \mu_B/\text{Co}$ which is the expected ordered moment when the e_g electrons are completely spin polarized. Our results are also consistent with the dHvA results which show a lot of dHvA branches derived from the cross-sections of FSs in the k_x - k_y planes [25].

As seen in Fig. 3(j), the γ band has a very narrow peak just below E_F . Such a very narrow peak just below E_F was observed by high-resolution spin-integrated photoemission spectroscopy using the Xe I α line below T_C [32]. Sato *et al.* [32] interpreted the peak structure as evidence for the occupied minority spin state around the R point, supported by their band-structure calculation results. Our high-resolution SARPES results, however, show that the peak structure is observed at k_F of the minority spin hole band around the Γ point. Note that the minority spin hole band around the Γ point cannot be attributed to a surface band because the band shows dispersion with the periodicity of the bulk Brillouin zone along the k_z direction, as shown as the intense band near E_F (see Supplemental Material [39]). In addition, a previous study on the surface of CoS₂(100) has shown that the surface bands are located between $E - E_F = -0.7$ and -0.2 eV along the ΓX direction [40], which supports that the δ band is not to be interpreted as a surface band. For understanding the minority spin bands around the Γ point, we analyze a more detailed comparison of our experimental spectra with the theoretical band structure, as discussed below.

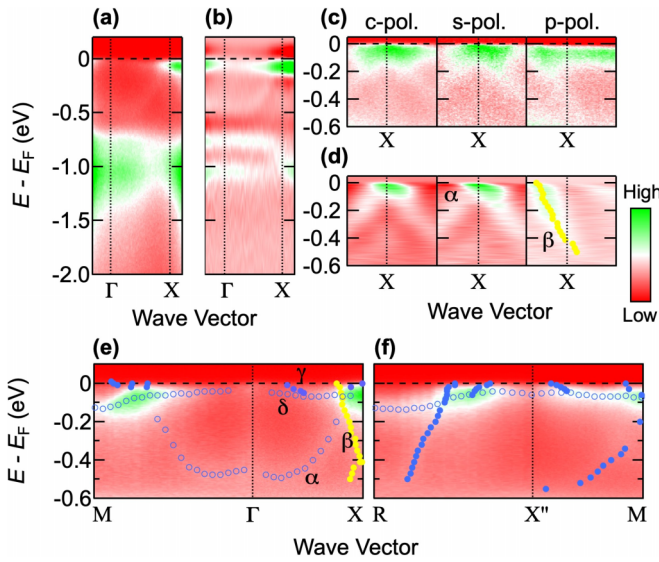


FIG. 2. (a) Angle-resolved photoemission spectroscopy (ARPES) intensity map as a function of energy up to E_F and wave vector. (b) Second derivative of ARPES intensity map in (a) with respect to energy. (c) Polarization-dependent ARPES intensity map around the X point: (left) circularly polarized light, (middle) s -polarized light, and (right) p -polarized light. (d) Second derivatives of ARPES intensity maps in (c) with respect to wave vector. Yellow filled circles show momentum distribution curve (MDC) peak positions estimated from the right panel in (c). (e) and (f) ARPES intensity maps along the $M\Gamma X$ and the $RX''M$ lines, respectively, overlaid with plots showing peak positions of energy distribution curves (EDCs; empty circles) and momentum distribution curves (MDCs; filled circles). Yellow filled circles are the same as in (d) but folded with respect to the X point.

C. Spin-dependent electron correlation

Figure 4(a) shows the theoretical band structure obtained from GGA with spin-orbit coupling (SOC) calculations with exchange reduced to 74%. The theoretical band structure without the exchange reduction is shown in the Supplemental Material [39]. The E_F position is determined to conserve the number of electrons. For the exchange-reduced band structure, the total moment is calculated to be $0.83 \mu_B/\text{Co}$, which is in good agreement with the experimental value [36]. From the correspondence between the theoretical and experimental total moments, it is appropriate to compare our ARPES and SARPES data with the exchange-reduced band structure. Note that, even though SOC leads to small additional band splittings, we discuss orbital character in terms of projection on l , m , and s quantum numbers which is still useful.

For the majority spin bands, the overall band structure calculated within GGA + SOC is in line with that obtained by ARPES shown in Fig. 2. For example, along the ΓX line, the α and β bands correspond to a band with a bottom at $E - E_F \sim -0.55$ eV at the Γ point and correspond to a light hole band crossing E_F , respectively. Furthermore, the orbital character of the α band is the d_{z^2} orbital, while the β band is mainly characterized by $d_{x^2-y^2}$ orbital character, based on the correspondence with the theoretical band structure. Note that, due to the distortion of the CoS_6 octahedra,

these two e_g orbitals are not degenerate. The difference of the orbital characters causes the polarization dependence of the ARPES intensity maps obtained around the X point shown in Figs. 2(c) and 2(d). For the minority spin bands, the γ band corresponds to a minority spin band whose bottom touches E_F in the middle of the ΓX line in the exchange-reduced band structure.

To further discuss the correspondence between the experimental spectra and the theoretical band structures, we compare the band structures and shapes of the FSs obtained by ARPES and by the exchange-reduced theoretical band structure. As shown in Figs. 4(c) and 4(d), the bands α , β , γ , and δ obtained from ARPES measurements can be assigned to the bands obtained from the GGA calculations. As shown in Fig. 4(c), we observed five FSs: α , β , γ , a pocket around the X' point, and a pocket around the M point in the cut P1, as mentioned above. In Fig. 4(d), we show the theoretical energy contour lines. The energy contour lines were assigned to the experimentally observed FSs based on correspondence of characteristics of the theoretical band structures with those of the experimental band structures; for instance, both the experimental contour line and the theoretical one which are assigned to FS γ are produced by a minority spin hole band. Comparing Figs. 4(c) with 4(d), squarelike contour lines corresponding to β and trapezoidal contour lines corresponding to the pocket around the X' point have characteristic shapes corresponding to those observed by ARPES. This agreement of the theoretical and experimental FSs indicates that the overall electronic structure can be roughly understood by the GGA calculation.

However, there is a deviation of our experimental band structure from our theoretical one in terms of effective mass. Figures 5(a)–5(d) show comparisons of the ARPES intensity maps along the ΓX line and the band structure calculated within GGA. The band widths of the experimentally observed majority spin bands (α , β) are well explained by the GGA calculations, while the band width of the γ band observed with 7 eV laser shown in Fig. 5(c) is much smaller than that obtained from the GGA calculations shown in Fig. 5(d). Estimating the effective mass of the γ band from quadratic curve fitting, the experimental effective mass was found to be >5 times larger than that of the GGA calculations. This suggests the magnitude of electronic correlation in CoS_2 is strongly dependent on the spin character.

To rigorously discuss the spin dependence of electron correlations, bands with identical orbital character but different spin characters must be compared because the orbital character-dependent contribution of electron correlations must be eliminated. We show the ARPES intensity map along the MR line overlaid with band plots showing the peak positions and show the theoretical bands in Figs. 5(e) and 5(f), respectively. The ε and ζ bands have the same orbital character, mainly $d_{x^2-y^2}$, but have opposite spin. In the theoretical band structure, the ε and ζ bands split at the R point due to SOC, which was not observed by ARPES in which the energy resolution was 20 meV. Focusing on the effective mass, the slope at k_F of the observed ε band is much larger than that of the calculated ε' and ε'' bands. This deviation can be attributed to mass renormalization of the theoretical ε' and ε'' bands due to a correlation effect. On the other hand, the

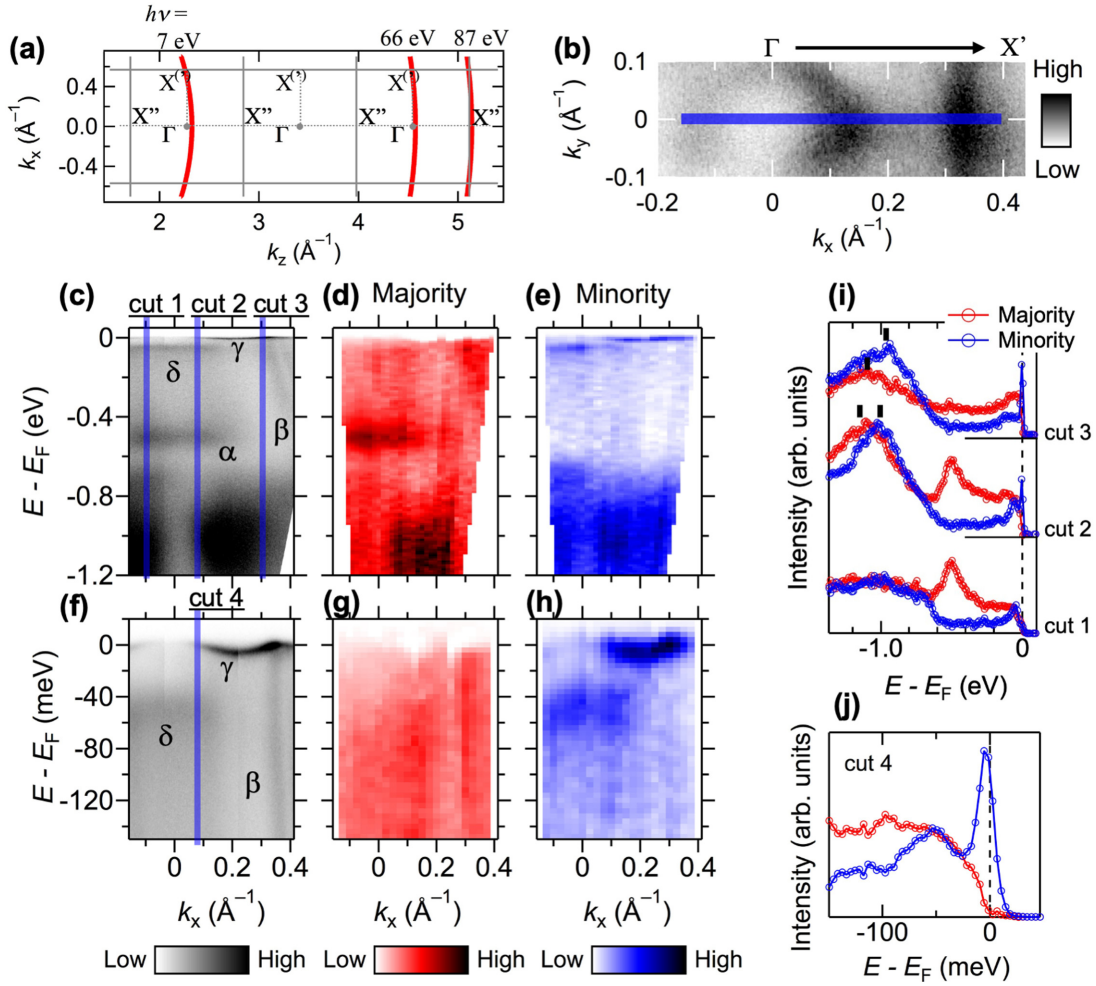


FIG. 3. (a) Two-dimensional Brillouin zone (gray lines) showing estimated measured k positions for the states near E_F (red curves) for each photon energy. (b) Angle-resolved photoemission spectroscopy (ARPES) intensity map of the Fermi surface (FS) as a function of k_x and k_y , measured by 7 eV laser. The FS is obtained with an energy-integration window of ± 1 meV. (c) ARPES and (d) spin- and angle-resolved photoemission spectroscopy (SARPES) majority spin bands and (e) SARPES minority spin bands intensity maps as a function of energy to E_F and k_x . (f)–(h) Same as (c)–(e) but measured in the vicinity of E_F . (i) and (j) Spin-resolved energy distribution curves (EDCs) at k points corresponding to the blue shaded line cuts in (c) and (f). Black solid markers in (i) indicate peak positions of the structure around -1 eV in the majority and minority spin spectra.

band width of the ζ band is larger than that of the ζ' and ζ'' bands. From the point of view of a tight-binding model, a wider bandwidth indicates a smaller effective mass. This suggests that the correlation of the minority spin electrons is larger than that of the majority spin electrons.

Here, we quantitatively compare the magnitude of the spin-dependent electronic correlation of CoS_2 with that of typical ferromagnets. For the electron bands around the Γ point of Ni (110), $\eta_\uparrow/\eta_\downarrow$ was estimated to be 1.6, where η_σ is a mass enhancement factor defined by $\eta_\sigma = m_\sigma^*/m_b$ [index σ indicates majority (\uparrow) or minority (\downarrow) spin state], where m_σ^* and m_b are effective masses given by ARPES and by GGA calculation, respectively [20]. For the exchange-split electron bands around the R point of CoS_2 (namely, the ε and ζ bands), $\eta_\uparrow/\eta_\downarrow$ was estimated to be $1.0/2.6 = 0.38$, where we assume that the effective mass of the ζ band is inversely proportional to the bandwidth.

These quantitative estimates are summarized in Table I. From Table I, we make two observations: (i) The mass renor-

malization of the minority spin band in CoS_2 is larger than that of the majority spin band, while in Ni, the relation of the mass renormalizations is inverse. (ii) The ratio of η_\uparrow and η_\downarrow of CoS_2 , $(\eta_\uparrow/\eta_\downarrow)^{-1} = 2.6$, is much larger than that of Ni(110), 1.6. This leads us to suspect that the near- E_F electronic structure constituted by unrenormalized majority spin bands and the large mass renormalization of minority spin bands are one of the characteristic features of a nearly HMF. A study on the HMF CrO_2 reported a similar result that the majority spin t_{2g} bands can be well reproduced by LSDA calculation with $U_{\text{eff}} < 1$ eV, although minority spin bands cannot be captured by the calculations because no minority spin t_{2g} band is observed below E_F for CrO_2 [16,19]. However, it has been reported that minority spin bands of CrO_2 are broadened by increasing thermal fluctuations due to a correlation effect [18]. This suggests strong correlation for the minority spin electrons, like the case of CoS_2 .

In a previous study of CoS_2 using SXARPES, the large spin-dependent electron correlation as observed in this paper

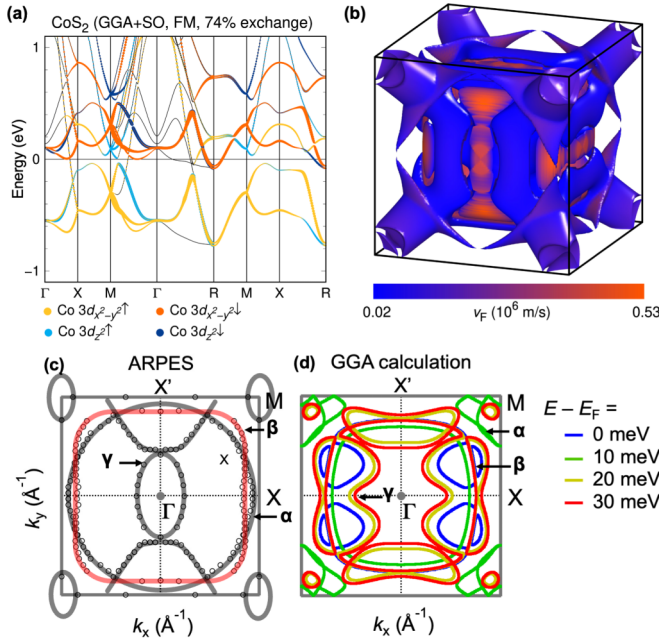


FIG. 4. Electronic structure of CoS₂ in ferromagnetic (FM) state determined with generalized gradient approximation (GGA) + spin-orbit coupling (SOC) exchange correlation functional. (a) Band structure calculated with exchange splitting reduced to 74%. Both majority and minority bands are crossing E_F . (b) Corresponding Fermi surface (FS) with majority and minority FS sheets. (c) Experimentally obtained k_F plots, same as Fig. 1(g). The thick shaded lines are guides for the eye. (d) Theoretical contour plots at $E - E_F = 0$ meV (blue; corresponding to FS), $E - E_F = 10$ meV (green), $E - E_F = 20$ meV (yellow), and $E - E_F = 30$ meV (red), calculated within GGA.

was not mentioned [33]. Along the XR direction, the k_F of the ε band is estimated to be $\sim 0.2\pi/a$ away from the R point in the previous study, while that in this paper is estimated to be $0.5\pi/a$, as shown in Fig. S6 in the Supplemental Material [39]. A reason for the observed smaller k_F in SXARPES is due to the difference in the magnitude of the exchange splitting. In the SXARPES results, the bottom of the band corresponding to the ζ band is ~ -0.65 eV, while in our ARPES results, it is estimated to be -0.6 eV. Since this difference can be attributed to the difference in the magnitude of the exchange splitting, the energy of the bottom of the ε band is on the high binding energy side with an energy scale comparable with that of the energy difference. Therefore, a larger k_F was obtained in our ARPES than the k_F estimated in the SXARPES study. It is still unclear why this difference in exchange splitting occurred, but one possibility is that it was due to sample dependency; calculations by Wu *et al.* [41] reported that a slight shift in the position of S can change the magnitude of the exchange splitting.

Based on our SARPES and band calculation results, the effective mass of the observed minority spin bands along the MR line is renormalized significantly, while that of the observed majority spin bands is rather smaller than that estimated from our GGA calculation. Such mass renormalization only for the minority spin electrons has been investigated as spin-dependent electronic correlation in studies on typical fer-

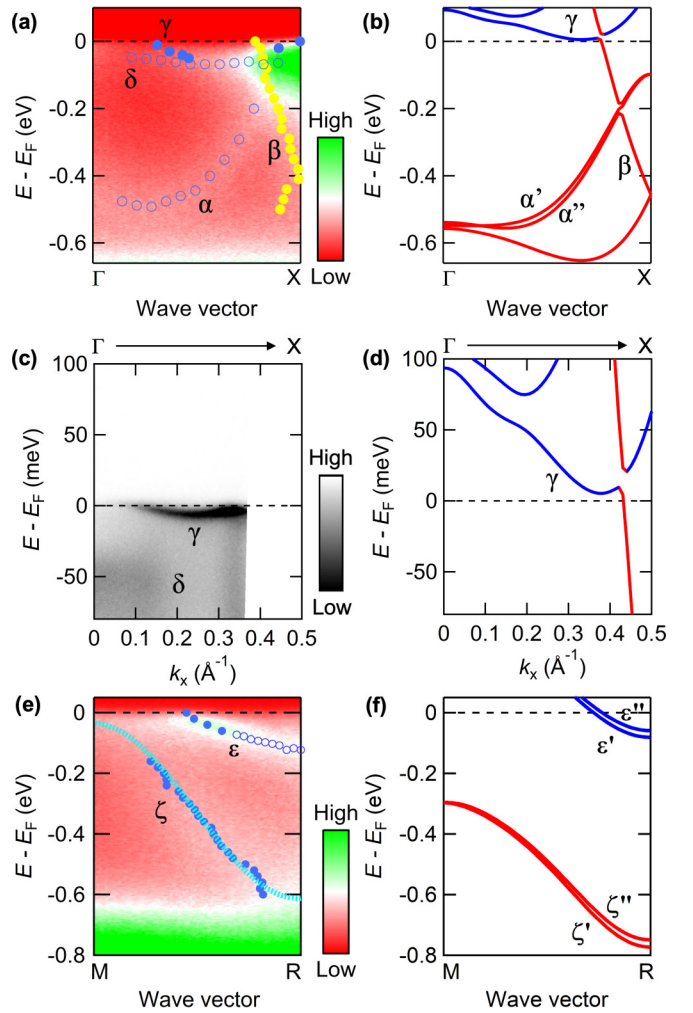


FIG. 5. Comparison of our experimental angle-resolved photoemission spectroscopy (ARPES) results with band structures calculated within generalized gradient approximation (GGA). (a) ARPES intensity map taken by synchrotron light along the ΓX direction with peak positions of energy distribution curves (EDCs; blue empty circles) and momentum distribution curves (MDCs; blue and yellow filled circles), same as Fig. 1(e). (b) Band structure along the ΓX direction obtained from GGA + spin-orbit coupling (SOC) calculations with exchange splitting reduced to 74%. Red and blue colors indicate the projected majority and minority spin character, respectively. (c) Same as (a) but taken by 7 eV laser. (d) Same as (b) but enlarged near E_F . (e) Same as (a) but taken along the MR direction. The light blue dotted line is the curve of the ζ band fitted with a cosine function to estimate the bandwidth. (f) Same as (b) but for the MR direction.

romagnetic metals [20–22]. One of the studies implies that the imaginary part of the self-energy Σ of Co $3d$ bands indicates a spin dependence [22]. There, although the electronic states of Co obtained by SARPES measurements cannot be explained by a LSDA + U calculation, which is like our findings, their spectra calculated by LSDA + DMFT within the one-step model improve the description of the experimental photoemission data. This suggests that the deviation of our experimental results from our theoretical band structure can be understood by introducing DMFT.

TABLE I. Effective mass (m^*) compared with the mass given by the GGA calculation (m_b) and the spin-dependent mass renormalization factor which is defined by the ratio between the effective mass for the majority spin (η_\uparrow) and that for the minority spin (η_\downarrow).

		$\eta_\sigma \equiv m_\sigma^*/m_b$ experiment	$\eta_\uparrow/\eta_\downarrow$	$\eta_\sigma \equiv m_\sigma^*/m_b$ DFT + DMFT	$\eta_\uparrow/\eta_\downarrow$
CoS ₂	Majority	1.0	1.0/2.6 = 0.38	1.2	0.70
	Minority	2.6		1.7	
Ni [20]	Majority	2.2	1.6		
	Minority	1.4			

Note that the spin-dependent electronic correlation is different from an orbital-dependent correlation discussed for iron-based superconductors. For the case of K_xFe_{2-y}Se₂, the magnitude of electronic correlations depends on the orbital character of Fe 3d [42]. For the case of the e_g bands in CoS₂, the magnitude of electronic correlations depends on the spin because the band shape of the calculated e_g^\uparrow and e_g^\downarrow bands is the same, and splitting them by an exchange interaction does not change the orbital character.

D. DMFT investigation

We performed DFT + DMFT calculations to investigate the spin-dependent renormalization beyond GGA. Technical details are summarized in Appendix C. Figure 6 shows the temperature dependence of the ferromagnetic moment M and the inverse of the ferromagnetic susceptibility $1/\chi$ for $J = 1.0$ eV and $U = 4$ eV. From the linear fitting of $1/\chi$, T_C was determined to be 401 K, which is larger than the experimental value of 122 K. If we consider that DFT + DMFT calculations with density-density interactions tend to overestimate T_C [43], we can consider this parameter set a reasonable choice. Also, the magnetic moment at a low temperature far below T_C was $0.90 \mu_B/\text{Co}$ which is in good agreement with the experimental value, $0.93 \mu_B/\text{Co}$ [25]. Numerical results for different parameter sets are provided in the Supplemental Material [39].

Figure 7 shows the single-particle excitation spectrum calculated within DFT + DMFT for $T/T_C = 0.58$. In Figs. 7(a) and 7(b), the t_{2g} bands split into majority spin bands and

minority spin bands, although the magnitude of splitting energy is not as large as that calculated within DFT + GGA [10]. The top of the majority spin t_{2g} bands has almost the same energy as that of the minority spin t_{2g} bands, while the bottom of the majority spin t_{2g} bands is ~ 0.3 eV lower than that of the minority spin t_{2g} bands. This difference of band width produces finite spin polarization in the density of states (DOS) of the t_{2g} bands. The spin polarization was observed by our SARPES measurements as an energy splitting of the majority spin energy distribution curve (EDC) and minority spin one, as shown in Fig. 3(i). While energy splitting of the t_{2g} bands estimated by GGA calculations is too large to explain the spin splitting observed by SARPES, DFT + DMFT calculations improve the description of the spin splitting of the t_{2g} bands.

As for the e_g bands, the correspondence between experimental and theoretical spectral functions has been improved. Along the ΓX line, two majority e_g bands cross E_F in the theoretical spectral functions: a large hole band around the Γ point and a small hole band near the X point. These bands produce two FSs closed around the Γ point with the majority spin character in the $\Gamma X M X'$ plane, as shown in Fig. 7(c). For the minority spin character, as shown in Fig. 7(d), unsharp trapezoidal FSs near the X point are also reproduced. In the $X'' M R M$ plane, the theoretical calculations show that a closed FS is located around the X'' point, as shown in Fig. 7(f). This FS corresponds to the circular FS observed by ARPES around the X'' point shown in Fig. 1(f), although the FS does not appear in GGA calculations [Fig. 4(b)]. For the minority spin states, the ε band touches E_F at the R point in the theoretical spectral function, which produces an electron pocket as shown in Fig. 7(g). In our ARPES intensity maps of the FS shown in Fig. 1(d), intensity at the R point is not so large because the bottom energy of the ε band is lower than that calculated within DFT + DMFT.

The DFT + DMFT calculations have improved the theoretical description of spin-dependent electron correlation. We compare the band dispersions along the MR line calculated within DFT + DMFT with those observed by ARPES, as shown in Fig. 8. In DFT + DMFT, the bandwidths of both ε and ζ bands are reduced compared with those of the GGA calculations. This can be interpreted as the increase in the effective mass due to the electronic correlation effects. Focusing on the magnitude of the bandwidth reduction compared with the GGA calculations, the bandwidth of the ζ band is reduced by 20%, while for the ε band, it is reduced by 45%. This spin-dependent reduction of the bandwidth is a result which better explains the spin-dependent electron correlation effects observed in the spectral function obtained by ARPES.

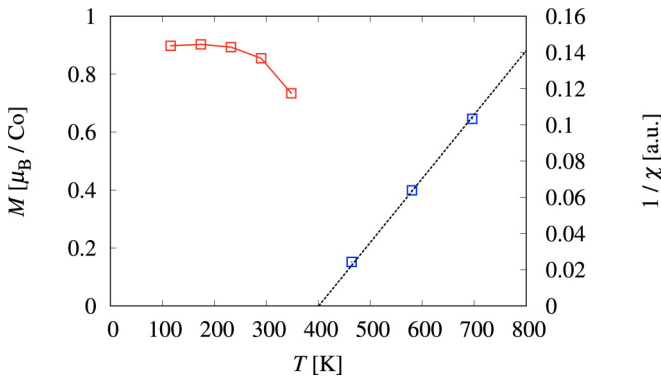


FIG. 6. Magnetic moment M (red squares) and inverse of the ferromagnetic susceptibility $1/\chi$ (blue squares) as a function of temperature, obtained dynamical mean-field theory (DMFT) calculations for $U = 4.0$ eV, $J = 1.0$ eV. T_C was determined from a linear fit of $1/\chi$ by the condition $1/\chi = 0$.

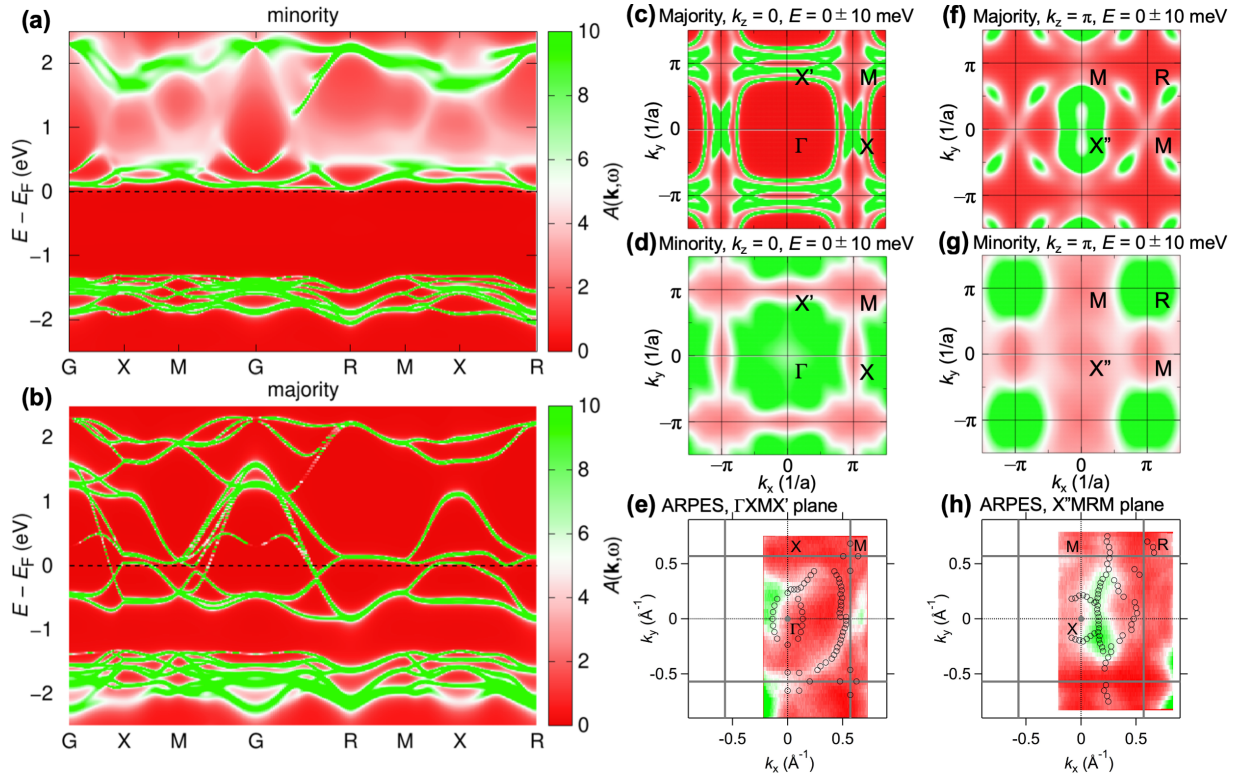


FIG. 7. The single-particle excitation spectrum for $T/T_C = 0.58$, $U = 4$ eV, and $J = 1.0$ eV for (a) the majority spin and (b) the minority spin calculated within density functional theory (DFT) + dynamical mean-field theory (DMFT). Momentum dependence of the zero-energy spectral functions in the $\Gamma XMX'$ plane in a 20 meV energy window for (c) the majority spin and (d) the minority spin calculated within DFT + DMFT and (e) obtained by angle-resolved photoemission spectroscopy (ARPES). (f)–(h) Same as (c)–(e) but in the $X'MRM$ plane.

Although the DFT + DMFT yields considerable improvement on the spin-dependent correlations, there are still quantitative deviations from the ARPES results. Figure 8 indicates that the ε band is in quite good agreement, while the bandwidth is underestimated by 0.1 eV for the ζ band. Additionally, the mass enhancement factor $\eta_\sigma \equiv m_\sigma^*/m_b$ for the minority spin band is estimated to be 1.7 in DFT + DMFT, while it is 2.6 in the experiment, as summarized in Table I. This deviation indicates that DFT + DMFT underestimates the correlation effects. This implies that correlations beyond DMFT play a role in the spin-dependent renormalization in CoS₂, which will be discussed in Sec. III F.

E. Temperature dependence

In Fig. 9, we examine the temperature evolution of the ARPES spectra. In Fig. 9(a), the spectral intensity of the δ band gets broader rapidly with increasing temperature up to $T_C (= 122$ K). Concomitantly, the β and γ bands are relatively enhanced. Except for the broadening, the band structure does not change significantly with increasing temperature. Moreover, from the EDCs shown in Figs. 9(b) and 9(c), although the peak structure at E_F gets broader rapidly, as seen in the ARPES intensity maps, the peak structure does not disappear even above T_C . From wide spectra corresponding to the Co 3d (t_{2g} and e_g) bands shown in Fig. 9(d), a peak structure corresponding to the α band shifts rapidly by +0.16 eV through T_C . Note that a temperature cycle of the measurements was

conducted to make sure that it is an intrinsic behavior, and not due to surface aging. Based on our SARPES results which demonstrate that the α and β (γ and δ) bands are the e_g^\uparrow (e_g^\downarrow) bands, the temperature dependence of the ARPES spectra demonstrates that the e_g^\uparrow and e_g^\downarrow bands are not degenerate even above T_C . This suggests that the origin of the demagnetization of CoS₂ is not Stoner damping but vanishing of the ferromagnetic long-range order by spin fluctuations, as in the case of iron [44,45].

In a previous spin- and angle-integrated photoemission study, the broadening of the near- E_F peak was interpreted as a change from the ferromagnetic electronic structure to the paramagnetic one, that is, as damping of the exchange splitting [32]. However, by our spin- and angle-resolved measurements, we identified that the exchange splitting remains above T_C , although the magnitude of the splitting reduced slightly. Therefore, the broadening of the δ band is rather attributed to a reduction of lifetime of the minority spin electrons. Figure 9(e) shows the temperature evolution of the width of the spectral peak at E_F (ΔE) shown in (c). Here, ΔE shows the T^2 dependence below T_C but deviates from the T^2 curve above T_C . The temperature evolution is nicely in line with that of the resistivity [25]. The fact that a deviation from the T^2 dependence of ΔE occurs at T_C of the bulk CoS₂ sample is consistent with the scenario that the δ band is a bulk rather than a surface band. The lifetime of the minority spin electrons (τ) corresponds to $1/\Delta E$ which rapidly increases below T_C , as shown in Fig. 9(f). Because the rapid broadening is

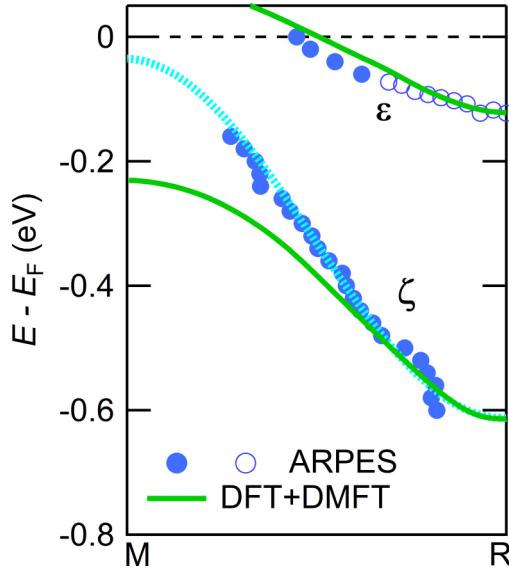


FIG. 8. Comparison of our angle-resolved photoemission spectroscopy (ARPES) results with the spectral function maxima calculated within density functional theory (DFT) + dynamical mean-field theory (DMFT). Blue empty (filled) circles show the peak positions of energy distribution curves (EDCs) [momentum distribution curves (MDCs)]. Light blue dotted line is the curve of the ζ band fitted with a cosine function. Solid green lines show the peak position of the single-particle excitation spectra calculated within DFT + DMFT, which are shifted so that the energy at the R point matches the experimental value.

characterized by T_C , it is found that scattering by magnetic fluctuations is a dominant factor contributing to the broadening of the near- E_F peak and the increase of the resistivity. Furthermore, the rapid broadening is significant for the δ band which is highly mass renormalized by correlations. This suggests that electron-electron scattering due to Coulomb interaction is also an indispensable factor contributing to the temperature dependence of the resistivity.

Here, we discuss prospects for realizing a half-metallic electronic structure at room temperature. The thermal broadening is quite like that predicted by DMFT calculations for HMFs [13,46–49]. DMFT calculations have demonstrated that, by thermal fluctuations, the spectrum of the electronic states for either one of the spin states forming a gap at E_F is broadened and has a finite value at E_F . This state emerging near E_F as a result of thermal fluctuations is called a nonquasiparticle (NQP) state, which has been observed experimentally as breaking of the half-metallicity in CrO_2 and Co_2MnSi [17,18,49]. These facts suggest that, although spin-dependent correlations may be a common characteristic of HMFs, as discussed above, electronic correlations break the half-metallicity at finite temperature, unfortunately. Furthermore, our results demonstrate that the e_g^\uparrow bands are well-described by a one-electron picture despite the $3d$ nature, which can be another remarkable feature specific to HMFs observed in CrO_2 [19]. This indicates that realizing weak

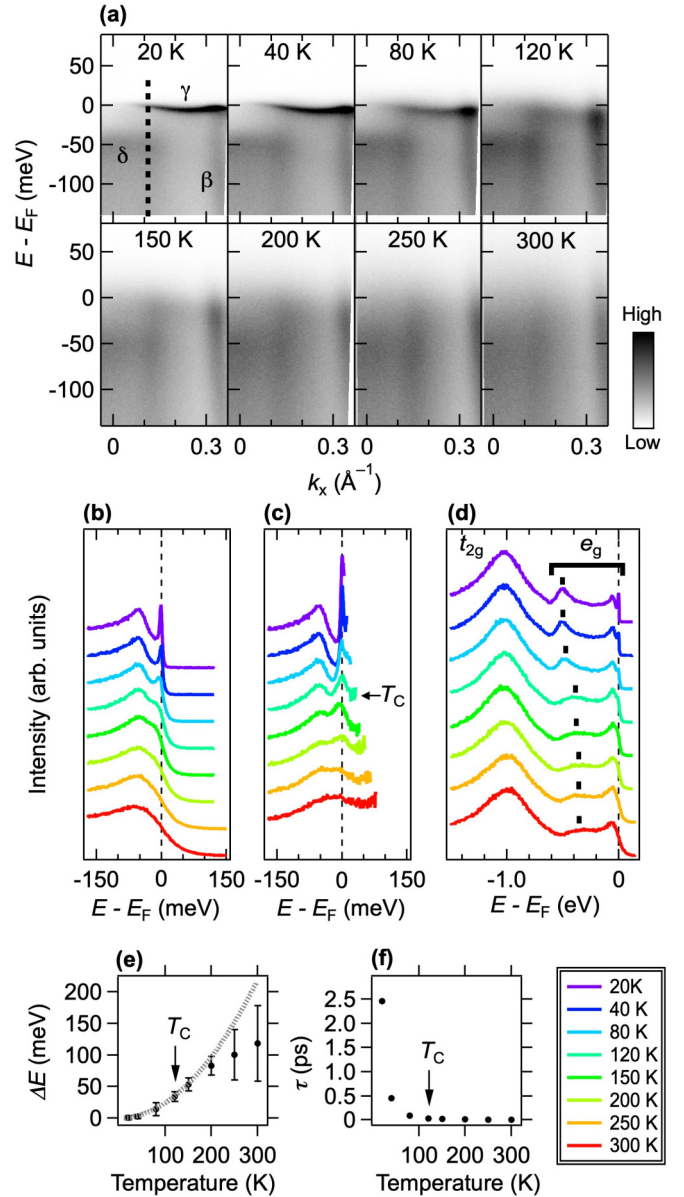


FIG. 9. (a) Temperature dependence of the angle-resolved photoemission spectroscopy (ARPES) intensity map along the ΓX line measured by 7 eV laser. (b) and (c) Energy distribution curves (EDCs) at a k_x point marked by the dotted line in (a) and those divided by the Fermi function at measured temperatures which is convoluted with a 6 meV Gaussian corresponding to the energy resolution of the measurement. The EDCs are normalized by their intensity at -150 meV. (d) EDCs at a k_x point marked by the dotted line in (a). The EDCs are normalized by the peak height at 1.0 eV. Black thick markers show positions of the structure corresponding to the α band. (e) Temperature evolution of the width of the spectral peak at E_F (ΔE) shown in (c). The ΔE plots are obtained after subtracting the energy resolution of our measurement, 6 meV. The gray dotted line denotes a fit of $\Delta E = A + BT^2$, where A and B are fitting parameters, and T is the temperature, to the data in a temperature range of 20–120 K. (f) Temperature evolution of the lifetime (τ) of the minority spin electrons occupying the δ band, estimated by $\tau = \hbar/\Delta E$.

correlation in the majority spin electronic states might lead to discovery of HMFs. In this paper, we offer insight that spin-dependent electronic correlations are one of the most important factors that must be understood further for realizing a half-metallic electronic structure at higher temperatures.

F. Possible origins of the spin-dependent electronic correlations in CoS₂

The large spin-dependent electronic correlations in CoS₂ are also observed in half-metal CrO₂, as mentioned above, and may in fact be a correlation effect specific to HMFs. Therefore, the spin-dependent electronic correlations could originate from the difference in number between majority and minority spin electrons near E_F . The largest electron correlation term is $U \sum_{\alpha} n_{\alpha\uparrow} n_{\alpha\downarrow}$ where the subscripts $\alpha = d_{z^2}, d_{x^2-y^2}$ denote the orbital component. This term only contains electron interactions between electrons with the same orbital character. In half-metallic electronic states, the magnitude of DOS near E_F varies greatly depending on the spin. Therefore, diagrammatic contributions to the self-energy will reflect the asymmetry in the DOS of majority and minority carriers. This effect might lead to spin-dependent effective masses and could thus be responsible for a spin dependence of electronic correlations. This model is only relevant for half-metallic electronic states and might universally apply in HMFs.

Another candidate for the origin of spin-dependent electronic correlations could be the difference of magnitude of the d - p hybridization. A study of GGA calculations shows that the fraction of orbital components that constitute the DOS near E_F varies with the spin orientation [10]. The majority spin states consist of Co $3d$ and S $3p$ orbitals in comparable proportions, while the minority spin states consist almost entirely of Co $3d$ orbitals. This difference in magnitude of d - p hybridization could be observed as intensity difference in our ARPES measurements: As shown in Fig. 2, the intensity of the majority spin band is smaller than that of the minority spin band near E_F . Considering that the cross-section of S $3p$ electrons is smaller than that of Co $3d$ at this photon energy (see Supplemental Material [39]), it can be inferred that the majority spin e_g bands are more strongly hybridized with the S $3p$ bands. Also from the valence charge density, the wave function of the e_g^{\uparrow} electrons is extended along the Co-S direction, while that of the e_g^{\downarrow} electrons is more localized around the Co nucleus. This originates from the difference in number between majority and minority spin electrons. The difference of wave-function extent might be another origin of the spin-dependent electronic correlation in CoS₂.

These two scenarios both attribute the spin-dependent correlations to the spin-dependent DOS as a characteristic of HMFs. These processes are considered by the DFT + DMFT calculations, though it is difficult to conclude which process is dominant in CoS₂. On the other hand, quantitative deviations between theory and experiment discussed in Sec. IID imply the existence of other factors that are not included in the DFT + DMFT calculations. One possibility is electron-magnon interaction discussed in the context of the NQP state [13]. It has been shown by perturbation theory that the electron-magnon exchange interaction affects the low-energy states of the minority spin band, which could enhance the spin-dependent

effective mass. DMFT considers only local spin fluctuations, and the feedback from the ferromagnetic magnon is missing. We conclude that the large spin-dependent electronic correlations originate in the spin-dependence of DOS plus nonlocal effects such as electron-magnon interactions.

III. CONCLUSIONS

We have investigated the electronic structure of pyrite-type CoS₂ by synchrotron ARPES and high-resolution SARPES. Along the ΓX line, we observed localized bands around $E - E_F = -1$ eV and dispersive bands between -0.5 eV and E_F . The overall character of the observed bands is in good agreement with the Co $3d$ bands calculated within GGA. In addition, localized bands were observed near E_F . From our SARPES measurements, we unambiguously identified that the near- E_F bands had minority spin character, while the GGA calculations predict that an occupied minority spin band exists solely around the R point. The deviation of the experimental spectra from the theoretical band structure is roughly explained by reducing the exchange splitting of the e_g band in GGA calculations, demonstrating that the GGA calculations overestimated the exchange splitting of CoS₂. However, the modified band structure cannot explain the bandwidth of the minority spin bands, although the bandwidths of the majority spin bands are in line with the theoretical bandwidths. This can be interpreted because of a spin-dependent electronic correlation effect. The ratio of the mass enhancement factors $(\eta_{\uparrow}/\eta_{\downarrow})^{-1}$ was estimated to be 2.6, which is much higher than that of a typical ferromagnetic metal like Ni where $\eta_{\uparrow}/\eta_{\downarrow} = 1.6$. We performed DFT + DMFT calculations to unveil the origin of the large spin-dependent electronic correlations. DFT + DMFT improves the description of the SARPES spectra compared with GGA, but a quantitative deviation remains. The large effective mass of the minority spin band was still underestimated by the DFT + DMFT calculations. This result implies the importance of spatial correlations beyond DMFT for the anomalously large spin-dependent electronic correlations in half-metallic materials. From our temperature-dependent ARPES experiments, we observed a decoherence of the mass-renormalized minority spin electrons which is much more rapid than that of the majority spin band. The decoherence of the minority spin band is scaled by T_C of CoS₂, indicating that the decoherence originates from increase of scattering of the conducting minority spin electrons by magnetic excitations. From the variation of the e_g bands, the majority and minority spin bands are not damped even above T_C , as seen in Fe metal. This indicates that the thermal demagnetization in CoS₂ is due to spin fluctuations. Through our thorough electronic-structure study of nearly HMF CoS₂, we suggest that spin-dependent electronic correlations are an important factor which must be considered not only for understanding phenomena appearing in spin-polarized strongly correlated systems but also for designing half-metallic materials via theoretical calculations.

ACKNOWLEDGMENTS

The laser-based SARPES experiments were conducted at ISSP with the approval of ISSP (Proposals No. B248,

No. A182, and No. A177). Part of the ARPES experiments were performed under the Photon Factory Proposal No. 2016G667. This paper was partially supported by the Program for Promoting the Enhancement of Research Universities and a Grant-in-Aid for the Japan Society for the Promotion of Science (JSPS) Fellows (Grant No. 16J03208), and JSPS KAKENHI (Grants No. JP18K03484, No. 20K20522, No. 20H01853, No. 20K20522, No. 21H01041, No. 21H01003, No. 21H01041, and No. 21H01003) from the Ministry of Education, Culture, Sports, Science and Technology of Japan (MEXT). H.F. was supported by a Grant-in-Aid for JSPS Fellows. Part of the computations were carried out at the Supercomputer Center at the Institute for Solid State Physics, the University of Tokyo. This paper was supported by MEXT Leading Initiative for Excellent Young Researchers. We thank A. Ino for providing his ARPES analysis program. We thank M. Shimizu for help with the DFT to DMFT interface. H.F. thanks T. Taniuchi and K. Okazaki for giving H.F. time to advance this study.

APPENDIX A: SAMPLES AND PHOTOEMISSION MEASUREMENTS

Single crystals of CoS_2 were synthesized by the vapor transport method [25] and were used for ARPES and SARPES measurements. ARPES experiments were carried out at beamline BL-28A of the Photon Factory, KEK, using synchrotron radiation as the excitation light source. Circularly polarized light was used, except for the polarization-dependence ARPES measurements. The total energy and angular resolutions were set to ~ 20 meV and 0.3° (corresponding to ~ 0.02 Å), respectively. Here, E_F of the samples was calibrated by measuring a gold foil that was electrically connected to the samples. The data were taken at $T = 50$ K. Laser-based ARPES and SARPES experiments were performed at the Institute for Solid State Physics, The University of Tokyo [50]. The p -polarized light with $h\nu = 6.994$ eV was used to excite the photoelectrons. Photoelectrons were analyzed with a combination of a ScientaOmicron DA30L analyzer and a very-low-energy-electron-diffraction (VLEED)-type spin detector. The energy and angular resolutions were set to 6 meV and 0.3° (corresponding to ~ 0.005 Å) for spin-integrated ARPES and 10 meV and 1° (corresponding to ~ 0.02 Å) for SARPES, respectively. The base pressure was kept below 1×10^{-8} Pa. Calibration of E_F for the samples was achieved using a gold reference. The data were taken at $T = 40$ K, except for the temperature-dependence data in Fig. 7. Clean surfaces for all measurements were obtained by *in situ* cleav-

ing of the samples. The high structural quality of a sample (100) surface was verified by LEED, as shown in Fig. 1(a). The sample was magnetized along the in-plane [010] direction by bringing the sample close to a magnet at low temperature below T_C . The approximate magnitude of the magnetic field at the sample position was 600 Oe.

APPENDIX B: DATA PROCESSING

The experimental FS maps in Fig. 1 were obtained with an energy-integration window of ± 0.01 eV, and those in Fig. 3 were done with an energy-integration window of ± 1 meV around E_F . To obtain absolute values of spin polarization using the VLEED detector, we used the equation $P = (1/M_0 S_{\text{eff}})(I_+ - I_-)/(I_+ + I_-)$, where M_0 is the ratio of the remanent magnetization of the sample to the saturated magnetization, a calibration factor in terms of magnetic domain, $S_{\text{eff}} (= 0.25)$ is the effective Sherman function of the apparatus, and $I_{+(-)}$ is the intensity of the electrons reflected by the positively (negatively) magnetized target. Then we obtain the majority (I_\uparrow) and minority (I_\downarrow) spin spectra using $I_{\uparrow(\downarrow)} = [1 + (-)P](I_{\text{tot}}/2)$, where $I_{\text{tot}} = I_+ + I_-$ [51,52].

APPENDIX C: THEORETICAL CALCULATIONS

We performed DFT calculations for CoS_2 within the full-potential local orbital (FPLO) [53] basis, using the Perdew-Burke-Ernzerhof parameterization of the GGA exchange correlation functional [54]. We based our calculations on the pyrite structure of CoS_2 given in Ref. [36] with lattice constant $a = 5.539$ Å and space group $Pa\bar{3}$. Here, k meshes of $12 \times 12 \times 12$ in the first Brillouin zone were used. Using the FPLO projective Wannier functions [55], we constructed a 44-band tight-binding model including Co $3d$ and S $3p$ orbitals (the unit cell includes four formula units).

We performed the DMFT self-consistency calculations using DCORE [56] implemented on the TRIQS library [57,58]. Summations over k and ω_n are performed with $n_k = 8^3$ points and $n_{i\omega} = 4096$ points (for positive frequencies), respectively. The effective impurity problems were solved with the hybridization-expansion algorithm [59,60] of the continuous-time quantum Monte Carlo method implemented as CT-HYB-SEGMENT [61] on ALPSCORE library [62]. The ARPES spectra $A(k, \omega) = \text{Tr}(-1/\pi)\text{Im}\hat{G}(\omega + i0)$ were computed by the analytical continuation from the Matsubara frequency to the real frequency using the Padé approximation [63]. More information is available in the Supplemental Material [39].

- [1] S. A. Wolf, D. D. Awschalom, R. A. Buhrman, J. M. Daughton, S. von Molnár, M. L. Roukes, A. Y. Chtchelkanova, and D. M. Treger, Spintronics: a spin-based electronics vision for the future, *Science* **294**, 1488 (2001).
- [2] I. Žutić, J. Fabian, and S. Das Sarma, Spintronics: fundamentals and applications, *Rev. Mod. Phys.* **76**, 323 (2004).
- [3] H. Y. Hwang and S.-W. Cheong, Enhanced intergrain tunneling magnetoresistance in half-metallic CrO_2 films, *Science* **278**, 1607 (1997).

- [4] A. Gupta and J. Z. Sun, Spin-polarized transport and magnetoresistance in magnetic oxides, *J. Magn. Magn. Mater.* **200**, 24 (1999).
- [5] J. M. D. Coey and M. Venkatesan, Half-metallic ferromagnetism: example of CrO_2 , *J. Appl. Phys.* **91**, 8345 (2002).
- [6] M. Jourdan, J. Minár, J. Braun, A. Kronenberg, S. Chadov, B. Balke, A. Gloskovskii, M. Kolbe, H. J. Elmers, G. Schönhense *et al.*, Direct observation of half-metallicity in the Heusler compound Co_2MnSi , *Nat. Commun.* **5**, 3974 (2014).

- [7] Y. Ando, Spintronics technology and device development, *Jpn. J. Appl. Phys.* **54**, 070101 (2015).
- [8] R. A. de Groot, F. M. Mueller, P. G. van Engen, and K. H. J. Buschow, New Class of Materials: Half-Metallic Ferromagnets, *Phys. Rev. Lett.* **50**, 2024 (1983).
- [9] K. Schwarz, CrO₂ predicted as a half-metallic ferromagnet, *J. Phys. F: Met. Phys.* **16**, L211 (1986).
- [10] T. Shishidou, A. J. Freeman, and R. Asahi, Effect of GGA on the half-metallicity of the itinerant ferromagnet CoS₂, *Phys. Rev. B* **64**, 180401(R) (2001).
- [11] S. J. Hashemifar, P. Kratzer, and M. Scheffler, Preserving the Half-Metallicity at the Heusler Alloy Co₂MnSi(001) Surface: A Density Functional Theory Study, *Phys. Rev. Lett.* **94**, 096402 (2005).
- [12] Y.-W. Son, M. L. Cohen, and S. G. Louie, Half-metallic graphene nanoribbons, *Nature (London)* **444**, 347 (2006).
- [13] M. I. Katsnelson, V. Yu. Irkhin, L. Chioncel, A. I. Lichtenstein, and R. A. de Groot, Half-metallic ferromagnets: from band structure to many-body effects, *Rev. Mod. Phys.* **80**, 315 (2008).
- [14] R. J. Soulen Jr., J. M. Byers, M. S. Osofsky, B. Nadgorny, T. Ambrose, S. F. Cheng, P. R. Broussard, C. T. Tanaka, J. Nowak, J. S. Moodera *et al.*, Measuring the spin polarization of a metal with a superconducting point contact, *Science* **282**, 85 (1998).
- [15] Y. Ji, G. J. Strijkers, F. Y. Yang, C. L. Chien, J. M. Byers, A. Anguelouch, G. Xiao, and A. Gupta, Determination of the Spin Polarization of Half-Metallic CrO₂ by Point Contact Andreev Reflection, *Phys. Rev. Lett.* **86**, 5585 (2001).
- [16] H. Fujiwara, M. Sunagawa, K. Terashima, T. Kittaka, T. Wakita, Y. Muraoka, and T. Yokoya, Intrinsic spin polarized electronic structure of CrO₂ epitaxial film revealed by bulk-sensitive spin-resolved photoemission spectroscopy, *Appl. Phys. Lett.* **106**, 202404 (2015).
- [17] H. Fujiwara, M. Sunagawa, K. Terashima, T. Kittaka, T. Wakita, Y. Muraoka, and T. Yokoya, Observation of intrinsic half-metallic behavior of CrO₂ (100) epitaxial films by bulk-sensitive spin-resolved PES, *J. Electron Spectrosc. Relat. Phenom.* **220**, 46 (2017).
- [18] H. Fujiwara, K. Terashima, M. Sunagawa, Y. Yano, T. Nagayama, T. Fukura, F. Yoshii, Y. Matsuura, M. Ogata, T. Wakita *et al.*, Origins of Thermal Spin Depolarization in Half-Metallic Ferromagnet CrO₂, *Phys. Rev. Lett.* **121**, 257201 (2018).
- [19] F. Bisti, V. A. Rogalev, M. Karolak, S. Paul, A. Gupta, T. Schmitt, G. Güntherodt, V. Eyert, G. Sangiovanni, G. Profeta *et al.*, Weakly-Correlated Nature of Ferromagnetism in Nonsym-morphic CrO₂ Revealed by Bulk-Sensitive Soft-X-Ray ARPES, *Phys. Rev. X* **7**, 041067 (2017).
- [20] M. Higashiguchi, K. Shimada, K. Nishiura, X. Cui, H. Namatame, and M. Taniguchi, Energy band and spin-dependent many-body interactions in ferromagnetic Ni(110): a high-resolution angle-resolved photoemission study, *Phys. Rev. B* **72**, 214438 (2005).
- [21] J. Sánchez-Barriga, J. Fink, V. Boni, I. Di Marco, J. Braun, J. Minár, A. Varykhalov, O. Rader, V. Bellini, F. Manghi *et al.*, Strength of Correlation Effects in the Electronic Structure of Iron, *Phys. Rev. Lett.* **103**, 267203 (2009).
- [22] J. Sánchez-Barriga, J. Braun, J. Minár, I. Di Marco, A. Varykhalov, O. Rader, V. Boni, V. Bellini, F. Manghi, H. Ebert *et al.*, Effects of spin-dependent quasiparticle renormalization in Fe, Co, and Ni photoemission spectra: an experimental and theoretical study, *Phys. Rev. B* **85**, 205109 (2012).
- [23] H. S. Jarrett, W. H. Cloud, R. J. Bouchard, S. R. Butler, C. G. Frederick, and J. L. Gillson, Evidence for Itinerant *d*-Electron Ferromagnetism, *Phys. Rev. Lett.* **21**, 617 (1968).
- [24] H. Hiraka and Y. Endoh, Ferromagnetic transition of Heisenberg ferromagnetic metal of CoS₂—Static critical Properties, *J. Phys. Soc. Jpn.* **63**, 4573 (1994).
- [25] A. Teruya, F. Suzuki, D. Aoki, F. Honda, A. Nakamura, M. Nakashima, Y. Amako, H. Harima, M. Hedo, T. Nakama, and Y. Ōnuki, Large cyclotron mass and large ordered moment in ferromagnet CoS₂ compared with paramagnet CoSe₂, *J. Phys. Soc. Jpn.* **85**, 064716 (2016).
- [26] R. Yamamoto, A. Machida, Y. Moritomo, and A. Nakamura, Reconstruction of the electronic structure in half-metallic CoS₂, *Phys. Rev. B* **59**, R7793(R) (1999).
- [27] G. L. Zhao, J. Callaway, and M. Hayashibara, Electronic structures of iron and cobalt pyrites, *Phys. Rev. B* **48**, 15781 (1993).
- [28] S. K. Kwon, S. J. Youn, and B. I. Min, Itinerant ferromagnetism in half-metallic CoS₂, *Phys. Rev. B* **62**, 357 (2000).
- [29] L. Wang, T. Y. Chen, and C. Leighton, Spin-dependent band structure effects and measurement of the spin polarization in the candidate half-metal CoS₂, *Phys. Rev. B* **69**, 094412 (2004).
- [30] V. N. Antonov, O. V. Andryushchenko, A. P. Shpak, A. N. Yaresko, and O. Jepsen, Electronic structure, optical spectra, and x-ray magnetic circular dichroism in CoS₂, *Phys. Rev. B* **78**, 094409 (2008).
- [31] T. Takahashi, Y. Naitoh, T. Sato, T. Kamiyama, K. Yamada, H. Hiraka, Y. Endoh, M. Usuda, and N. Hamada, Para- to ferromagnetic phase transition of CoS₂ studied by high-resolution photoemission spectroscopy, *Phys. Rev. B* **63**, 094415 (2001).
- [32] T. Sato, S. Souma, K. Sugawara, K. Nakayama, S. Raj, H. Hiraka, and T. Takahashi, Xenon-plasma-light low-energy ultrahigh-resolution photoemission study of Co(S_{1-x}Se_x)₂ (*x* = 0.075), *Phys. Rev. B* **76**, 113102 (2007).
- [33] N. B. M. Schröter, I. Robredo, S. Klemenz, R. J. Kirby, J. A. Krieger, D. Pei, T. Yu, S. Stolz, T. Schmitt, P. Dudin *et al.*, Weyl fermions, fermi arcs, and minority-spin carriers in ferromagnetic CoS₂, *Sci. Adv.* **6**, eabd5000 (2020).
- [34] I. I. Mazin, Robust half metallicity in FexCo_{1-x}S₂, *Appl. Phys. Lett.* **77**, 3000 (2000).
- [35] C. Leighton, M. Manno, A. Cady, J. W. Freeland, L. Wang, K. Umemoto, R. M. Wentzcovitch, T. Y. Chen, C. L. Chien, P. L. Kuhns *et al.*, Composition controlled spin polarization in Co_{1-x}FexS₂ alloys, *J. Phys.: Condens. Matter* **19**, 315219 (2007).
- [36] P. J. Brown, K.-U. Neumann, A. Simon, F. Ueno, and K. R. A. Ziebeck, Magnetization distribution in CoS₂; is it a half metallic ferromagnet? *J. Phys.: Condens. Matter* **17**, 1583 (2005).
- [37] Y. Zhang, F. Chen, C. He, B. Zhou, B. P. Xie, C. Fang, W. F. Tsai, X. H. Chen, H. Hayashi, J. Jiang *et al.*, Orbital characters of bands in the iron-based superconductor BaFe_{1.85}Co_{0.15}As₂, *Phys. Rev. B* **83**, 054510 (2011).
- [38] M. Sunagawa, K. Terashima, T. Hamada, H. Fujiwara, T. Fukura, A. Takeda, M. Tanaka, H. Takeya, Y. Takano, M. Arita *et al.*, Observation of a hidden hole-like band approaching the Fermi level in K-doped iron selenide superconductor, *J. Phys. Soc. Jpn.* **85**, 073704 (2016).
- [39] See Supplemental Material at <http://link.aps.org/supplemental/10.1103/PhysRevB.106.085114> for additional details of the

- ARPES measurements and their evaluation including additional spectra, for a description of the DFT and DMFT calculations with additional results and for details of the determination of ferromagnetic ordering temperature and effective mass.
- [40] N. Wu, R. F. Sabirianov, W. N. Mei, Ya. B. Losovyj, N. Lozova, M. Manno, C. Leighton, and P. A. Dowben, The minority spin surface bands of $\text{CoS}_2(001)$, *J. Phys.: Condens. Matter* **21**, 295501 (2009).
- [41] N. Wu, Y. B. Losovyj, D. Wisbey, K. Belashchenko, M. Manno, L. Wang, C. Leighton, and P. A. Dowben, The electronic band structure of CoS_2 , *J. Phys.: Condens. Matter* **19**, 156224 (2007).
- [42] M. Yi, Z.-K. Liu, Y. Zhang, R. Yu, J.-X. Zhu, J. J. Lee, R. G. Moore, F. T. Schmitt, W. Li, S. C. Riggs *et al.*, Observation of universal strong orbital-dependent correlation effects in iron chalcogenides, *Nat. Commun.* **6**, 7777 (2015).
- [43] A. S. Belozerov, I. Leonov, and V. I. Anisimov, Magnetism of iron and nickel from rotationally invariant Hirsch-Fye quantum Monte Carlo calculations, *Phys. Rev. B* **87**, 125138 (2013).
- [44] E. Kisker, K. Schröder, W. Gudat, and M. Campagna, Spin-polarized angle-resolved photoemission study of the electronic structure of $\text{Fe}(100)$ as a function of temperature, *Phys. Rev. B* **31**, 329 (1985).
- [45] R. Kurzawa, K.-P. Kämper, W. Schmitt, and G. Güntherodt, Spin-resolved photoemission study of *in situ* grown epitaxial Fe layers on $\text{W}(110)$, *Solid State Commun.* **60**, 777 (1986).
- [46] L. Chioncel, E. Arrigoni, M. I. Katsnelson, and A. I. Lichtenstein, Electron Correlations and the Minority-Spin Band Gap in Half-Metallic Heusler Alloys, *Phys. Rev. Lett.* **96**, 137203 (2006).
- [47] V. Yu. Irkhin, M. I. Katsnelson, and A. I. Lichtenstein, Non-quasiparticle effects in half-metallic ferromagnets, *J. Phys.: Condens. Matter* **19**, 315201 (2007).
- [48] L. Chioncel, H. Allmaier, E. Arrigoni, A. Yamasaki, M. Daghofer, M. I. Katsnelson, and A. I. Lichtenstein, Half-metallic ferromagnetism and spin polarization in CrO_2 , *Phys. Rev. B* **75**, 140406(R) (2007).
- [49] L. Chioncel, Y. Sakuraba, E. Arrigoni, M. I. Katsnelson, M. Oogane, Y. Ando, T. Miyazaki, E. Burzo, and A. I. Lichtenstein, Nonquasiparticle States in Co_2MnSi Evidenced Through Magnetic Tunnel Junction Spectroscopy Measurements, *Phys. Rev. Lett.* **100**, 086402 (2008).
- [50] K. Yaji, A. Harasawa, K. Kuroda, S. Toyohisa, M. Nakayama, Y. Ishida, A. Fukushima, S. Watanabe, C. Chen, F. Komori *et al.*, High-resolution three-dimensional spin- and angle-resolved photoelectron spectrometer using vacuum ultraviolet laser light, *Rev. Sci. Instrum.* **87**, 053111 (2016).
- [51] P. D. Johnson, Spin-polarized photoemission, *Rep. Prog. Phys.* **60**, 1217 (1997).
- [52] M. Hoesch, T. Greber, V. N. Petrov, M. Muntwiler, M. Hengsberger, W. Auwärter, and J. Osterwalder, Spin-polarized Fermi surface mapping, *J. Electron Spectrosc. Relat. Phenom.* **124**, 263 (2002).
- [53] K. Koepnik and H. Eschrig, Full-potential nonorthogonal local-orbital minimum-basis band-structure scheme, *Phys. Rev. B* **59**, 1743 (1999).
- [54] J. P. Perdew, K. Burke, and M. Ernzerhof, Generalized Gradient Approximation Made Simple, *Phys. Rev. Lett.* **77**, 3865 (1996).
- [55] H. Eschrig and K. Koepnik, Tight-binding models for the iron-based superconductors, *Phys. Rev. B* **80**, 104503 (2009).
- [56] H. Shinaoka, J. Otsuki, M. Kawamura, N. Takemori, and K. Yoshimi, DCORE: integrated DMFT software for correlated electrons, *SciPost Phys.* **10**, 117 (2021).
- [57] M. Aichhorn, L. Pourovskii, P. Seth, V. Vildosola, M. Zingl, O. E. Peil, X. Deng, J. Mravlje, G. J. Kraberger, C. Martins, M. Ferrero, and O. Parcollet, TRIQS/DFPTOOLS: a TRIQS application for *ab initio* calculations of correlated materials, *Comput. Phys. Commun.* **204**, 200 (2016).
- [58] O. Parcollet *et al.*, TRIQS: A toolbox for research on interacting quantum systems, *Comput. Phys. Commun.* **196**, 398 (2015).
- [59] P. Werner, A. Comanac, L. de' Medici, M. Troyer, and A. J. Millis, Continuous-Time Solver for Quantum Impurity Models, *Phys. Rev. Lett.* **97**, 076405 (2006).
- [60] E. Gull, A. J. Millis, A. I. Lichtenstein, A. N. Rubtsov, M. Troyer, and P. Werner, Continuous-time Monte Carlo methods for quantum impurity models, *Rev. Mod. Phys.* **83**, 349 (2011).
- [61] H. Hafermann, P. Werner, and E. Gull, Efficient implementation of the continuous-time hybridization expansion quantum impurity solver, *Comput. Phys. Commun.* **184**, 1280 (2013).
- [62] A. Gaenko, A. E. Antipov, G. Carcassi, T. Chen, X. Chen, Q. Dong, L. Gamper, J. Gukelberger, R. Igarashi, S. Isakov *et al.*, Updated core libraries of the ALPS project, *Comput. Phys. Commun.* **213**, 235 (2017).
- [63] H. J. Vidberg and J. W. Serene, Solving the Eliashberg equations by means of N -point Padé approximants, *J. Low Temp. Phys.* **29**, 179 (1977).